Yabe and Ide *Progress in Earth and Planetary Science* (2018) 5:43
https://doi.org/10.1186/s40645-018-0201-x

Progress in Earth and Planetary Science

RESEARCH ARTICLE Open Access

Variations in precursory slip behavior resulting from frictional heterogeneity

Suguru Yabe[1*] and Satoshi Ide[2]

Abstract

Precursory seismicity is often observed before a large earthquake. Small foreshocks occur within the mainshock rupture area, which cannot be explained by simple models that assume homogeneous friction on the entire fault. In this study, we consider a frictionally heterogeneous fault model, motivated by recent observations of geologic faults and slow earthquakes. This study investigates slip behavior on faults governed by a rate- and state-dependent friction law. We consider a finite linear fault consisting of alternating velocity-weakening zones (VWZs) and velocity-strengthening zones (VSZs). Our model generates precursory slip before the mainshock that ruptures the entire fault, though the activity level of the precursory slip depends on the frictional parameters. We investigate variations in precursory slip behavior, which we characterize quantitatively by the background slip acceleration and seismic radiation, using parameter studies of the a value of the VWZs and VSZs. The results reveal that precursory slip is very small when VWZs are strongly locked and when VSZs consume only a small amount of energy during seismic slip. Precursory slip is significant around the stability boundary of the fault. Furthermore, the type of precursory slip (seismic or aseismic) is controlled by the amplitude of the frictional heterogeneity. Active foreshocks obeying an inverse Omori law associated with background aseismic slip can be interpreted as the nucleation of the mainshock, though this is different from classical nucleation because the monotonic increase in slip velocity is significantly perturbed by the occurrence of foreshocks. Frictional heterogeneity also affects interseismic slip behavior. Modeled variations in precursory slip behavior and interseismic activity can qualitatively explain the along-dip and among-subduction-zone variations in real seismicity patterns. Because even simple frictional heterogeneity produces complex seismicity, it is necessary to further investigate the slip behavior of frictionally heterogeneous faults, which could be utilized for modeling various real seismicity patterns.

Keywords: Rate- and state-dependent friction law, Frictional heterogeneity, Foreshock, Inverse Omori law, Dynamic nucleation

Introduction

An increase in seismicity, or foreshock activity, has long been recognized during the period before large earthquakes (e.g., Jones and Molnar 1979; Dodge et al. 1995; Abercrombie and Mori 1996; Bouchon et al. 2011, 2013). Foreshocks were also reported in recent megathrust earthquakes in subduction zones, such as the 2011 Tohoku-Oki earthquake in Japan and the 2014 Iquique earthquake in Chile, in association with slow slip around the eventual hypocenter of the mainshock (Ando and Imanishi 2011; Kato et al. 2012; Ito et al. 2013; Ruiz et al. 2014). Similar observations have been reported in rock fracture experiments, where local seismic sources are located within the aseismically slipping (nucleation) zone before slip occurs on the rock surface (McLaskey and Kilgore 2013). Foreshocks are considered to be driven by the nucleation process of the mainshock and therefore are expected to act as precursors to large earthquakes (Dodge et al. 1996; McGuire et al. 2005). On the other hand, the epidemic-type aftershock sequence (ETAS) model (Ogata 1988), which considers only mainshock-aftershock triggering, explains many of the statistical properties of foreshock activity, such as the inverse Omori law and Båth's law (Helmstetter and Sornette 2003a, 2003b); this suggests that foreshocks are generated by the usual mainshock-aftershock triggering

* Correspondence: syabe@jamstec.go.jp
[1]Department of Solid Earth Geochemistry, Japan Agency for Marine-Earth Science and Technology, 2-15, Natsushima-cho, Yokosuka, Kanagawa 237-0061, Japan
Full list of author information is available at the end of the article

Springer Open

© The Author(s). 2018 **Open Access** This article is distributed under the terms of the Creative Commons Attribution 4.0 International License (http://creativecommons.org/licenses/by/4.0/), which permits unrestricted use, distribution, and reproduction in any medium, provided you give appropriate credit to the original author(s) and the source, provide a link to the Creative Commons license, and indicate if changes were made.

mechanism (Helmstetter et al. 2003). However, the physical mechanism of foreshock generation remains poorly understood.

Recent findings in the field of slow earthquake studies emphasize the importance of fault heterogeneity. The existence of high-frequency seismic signals (tectonic tremors) suggests that a velocity-weakening (or slip-weakening) friction law governs fault behavior, whereas the sensitivity of tectonic tremors to small stress perturbations implies that a velocity-strengthening friction law controls the fault, assuming that the tremor rate is proportional to the slip velocity on the fault (Miyazawa and Brodsky 2008; Beeler et al. 2013; Ide and Tanaka 2014; Houston 2015; Yabe et al. 2015). Geologic observations also suggest that ancient plate boundary faults comprise a mixture of ductile matrix and brittle blocks (Fagereng and Sibson 2010; Fagereng et al. 2014; Ujiie et al. 2018). The hydraulic properties of geologic faults could also be heterogeneous (Wibberley and Shimamoto 2003), which would cause heterogeneous distributions of pore fluid pressure and effective normal stress.

The slip behavior of frictionally heterogeneous faults has been investigated in several studies. Dublanchet et al. (2013) and Yabe and Ide (2017) investigated the slip behavior of infinite-length planar and linear faults with periodic frictional parameter distributions, respectively. They reported a variety of slip behaviors, from seismic slip that ruptures only the velocity-weakening zone (VWZ) to seismic slip that ruptures the entire fault, including both the VWZ and velocity-strengthening zone (VSZ). Yabe and Ide (2017) documented slower deformation at the transition between two behaviors, which may correspond to slow earthquakes. In contrast, Skarbek et al. (2012) documented transitions from seismic to slow slip on a finite frictionally heterogeneous fault. Luo and Ampuero (2017) performed a thorough stability analysis of an infinite frictionally heterogeneous fault. Yabe and Ide (2018; hereafter YI18) reproduced aftershocks within the mainshock rupture area (e.g., Beroza and Zoback 1993; Woessner et al. 2006) by considering the partial rupture of a frictionally heterogeneous fault. Dublanchet et al. (2013) and YI18 reported foreshocks before the mainshock, though no previous study has investigated the causes of variations in foreshock activity.

Motivated by those observations, this study investigates the precursory slip behavior of a frictionally heterogeneous fault comprising VWZs and VSZs governed by a rate- and state-dependent friction (RSF) law (Dieterich 1979). We quantify the precursory slip behaviors from two perspectives: background aseismic slip velocity and seismic wave energy radiation. Parameter studies reveal that precursory slip behavior is dependent on the frictional parameters of the VWZs and VSZs, and intense precursory slip is observed around the stability boundary of the fault.

Methods/Experimental

As in YI18, this study investigates slip behavior on a finite linear fault governed by the RSF law (Dieterich 1979) in a two-dimensional (2D) antiplane elastic space (Fig. 1). The seismogenic zone on the fault consists of 70 cells, each of which comprises a paired VWZ and VSZ with a large VSZ at the edge. Outside of the modeled fault, it is assumed that the fault slips stably at plate velocity V_{pl}. The lengths of each VWZ-VSZ pair are 6 m and 2 m, which are discretized into 60 and 20 subfaults for numerical simulations, respectively. The system is bilaterally symmetric. The shear stress on the ith subfault, τ_i, is given by:

$$\tau_i = \tau_0 + \sum\nolimits_j K_{ij}\left(u_j - V_{\mathrm{pl}}t\right) - \frac{\mu}{2\beta}V_i, \tag{1}$$

where τ_0 is the ambient shear stress, u_j is the slip distance on the jth subfault, t is time, μ is the shear modulus, β is the shear wave velocity, and V_i is the slip velocity on the ith subfault. The last term is a radiation damping term (Rice 1993), and we consider only static stress interactions for kernel K_{ij} (Dieterich 1992). Interactions between seismic patches with a dynamic-stress kernel should show qualitatively similar behaviors to interactions with a static-stress kernel (Thomas et al. 2014).

Based on the RSF law, the shear stress on the ith subfault is also given:

$$\tau_i = \tau_0 + a_i\sigma \log\frac{V_i}{V_{\mathrm{pl}}} + b_i\sigma \log\frac{\theta_i}{\theta_{\mathrm{pl}}}, \tag{2}$$

where σ is the normal stress on the fault, θ_i is the state variable of the ith subfault, and θ_{pl} is the reference state variable at the plate velocity. We use the aging law of Dieterich (1979) in this study:

$$\frac{d\theta}{dt} = 1 - \frac{V\theta}{D_{\mathrm{c}}}, \tag{3}$$

where D_{c} is the characteristic slip distance. Taking the time derivatives of Eqs. (1) and (2), and equating them, yields:

Fig. 1 Model space of the numerical simulations. Only the left half of the model space is shown here because the system is bilaterally symmetric. Red and blue lines denote velocity-weakening zones (VWZs) and velocity-strengthening zones (VSZs), respectively. Cells (pairs of VWZ and VSZ) are numbered from #1 at the edge to #35 at the center of the fault. A wide VSZ is set at the edge of the model space. The region outside the model space is assumed to slip stably at the plate velocity

$$\left(\frac{\mu}{2\beta}+\frac{a_i\sigma}{V_i}\right)\frac{dV_i}{dt}=\sum\nolimits_j K_{ij}\left(V_j-V_{\mathrm{pl}}\right)-b_i\sigma\frac{\dot{\theta}_i}{\theta_i}. \quad (4)$$

Because τ_0 does not appear in Eq. (4), its value does not affect the slip behavior of the fault. The time evolutions of Eqs. (3) and (4) are solved by a time-adaptive Runge-Kutta-Fehlberg method (Fehlberg 1969; YI18).

We now describe how the frictional parameters of the RSF law are distributed. For the entire fault, the parameters b and D_c are set to uniform values of 0.002 and 10 μm, respectively. At the edge of the model space, a wide VSZ is imposed to avoid mathematical artifacts that result from evaluating the convolution in (4) using an FFT (Fig. 1). In this wide VSZ, $a = 0.010$. Constant a values are assigned to other VSZs and VWZs, which consist of seismogenic zones on the fault. We conducted a parameter study by changing the a value in the VWZs and VSZs. In the VWZs, a varies from 0.0002 to 0.0018 in increments of 0.0002; in the VSZ, we tested $a = 0.0021$ and the range $a = 0.0025$–0.0060 in increments of 0.0005.

In the remainder of this manuscript, we refer to the position along strike using our cell numbering convention: position #1 corresponds to the edge of the seismogenic zone and position #35 corresponds to the center. Seismicity for 1000 days has been calculated in each simulation, and the last 500 days are used for the following analysis to reduce biases related to transient behavior at the beginning of each set of calculations. We use the following values for other parameters: rigidity $\mu = 30$ GPa, shear wave velocity $\beta = 3$ km/s, effective normal stress $\sigma = 100$ MPa, and plate loading velocity $V_{\mathrm{pl}} = 10^{-9}$ m/s. These parameters yield a minimum nucleation size $L_b = \mu D_c/b\sigma$ of 1.5 m (Rubin and Ampuero 2005). The fault is discretized into subfaults, each with a size of 0.1 m, much shorter than the minimum length required for nucleation. The slip velocity discussed and presented in the following manuscript and figures is averaged within each cell (i.e., spatially averaged in 80 m regions) because we discuss the frictional heterogeneity on scales smaller than the sizes of large earthquakes. Because the system is bilaterally symmetric, only the left half of each fault is shown in the figures.

Results

Seismic cycle

Consistent with previous studies (e.g., Skarbek et al. 2012; Dublanchet et al. 2013; Luo and Ampuero 2017; Yabe and Ide 2017), we observed several different types of slip behavior in our parameter studies. The first is the "total seismic" regime, in which a mainshock event ruptures the entire seismogenic zone on the fault (parameter sets A-C in Fig. 2). Here, the slip behavior between mainshocks depends on the frictional parameter. In most cases, smaller stick-slip events occur, comprising seismic ruptures of one or more cells, but not all cells (parameter sets A and B in Fig. 2). The frequency of smaller events also varies with the frictional parameters. In some cases, seismic events do not occur between mainshocks except for slow slip events (parameter set C in Fig. 2). The second regime is the "partial seismic" regime, in which each cell shows stick-slip behavior but simultaneous slip does not occur across the entire seismogenic zone (parameter set D in Fig. 2). We also observe a "slow slip" regime where the entire seismogenic zone shows stick-slip behavior, though peak slip velocity does not reach seismic slip velocity, which is defined as 1 mm/s in this study (parameter set E in Fig. 2). The last regime is the "stable slip" regime, where stick-slip events are never initiated (parameter set F in Fig. 2).

We present the detailed slip behavior of frictionally heterogeneous faults on shorter timescales in Fig. 3. In the total seismic regime, slip velocity distributions on the fault are shown in a 20 s window around the mainshock (parameter sets A–C in Fig. 3). Slip velocity decelerates monotonically after the mainshock, whereas the preseismic behavior is less uniform. Although part of the fault is accelerated before the mainshock (i.e., the nucleation), its width depends on the frictional parameters. Furthermore, in Fig. 3 for parameter sets B and C, part of the fault accelerates to seismic slip velocity for a short period before the mainshock, which represents foreshocks. During the mainshock, the entire seismogenic zone simultaneously accelerates to seismic slip velocity. In the partial seismic regime (parameter set D in Fig. 3), individual cells are accelerated to seismic slip velocity but the accelerations themselves are not simultaneous; rather, we observe a migrating cell rupture with variable time delays between adjacent ruptures. In the slow slip regime (parameter set E in Fig. 3), cells are never accelerated to seismic slip velocity; instead, the rupture of the fault propagates slowly from the center of the seismogenic zone to the edge.

To assess the dependence of the four types of slip behavior on the frictional parameters, we measure the peak value of slip velocity V_{ave} averaged across the entire seismogenic zone (Fig. 4). The total seismic regime has a high peak slip velocity (~ 0.1 m/s) because the entire seismogenic zone simultaneously reaches seismic slip velocity. The total seismic regime is observed when $(b-a)\sigma$ in the VWZ (ξ_w) is large and $(a-b)\sigma$ in the VSZ (ψ_s) is small. On the other hand, when both ξ_w and ψ_s are large, the partial seismic regime has a lower peak average-slip velocity (~ 1 mm/s) because only a small part of the seismogenic zone slips seismically at one time. When ξ_w is small and ψ_s is large, stick-slip events are never initiated (i.e., the fault is in a stable slip regime). The slow slip regime is observed in a narrow parameter space between the total seismic regime and the stable slip regime, with smaller ξ_w.

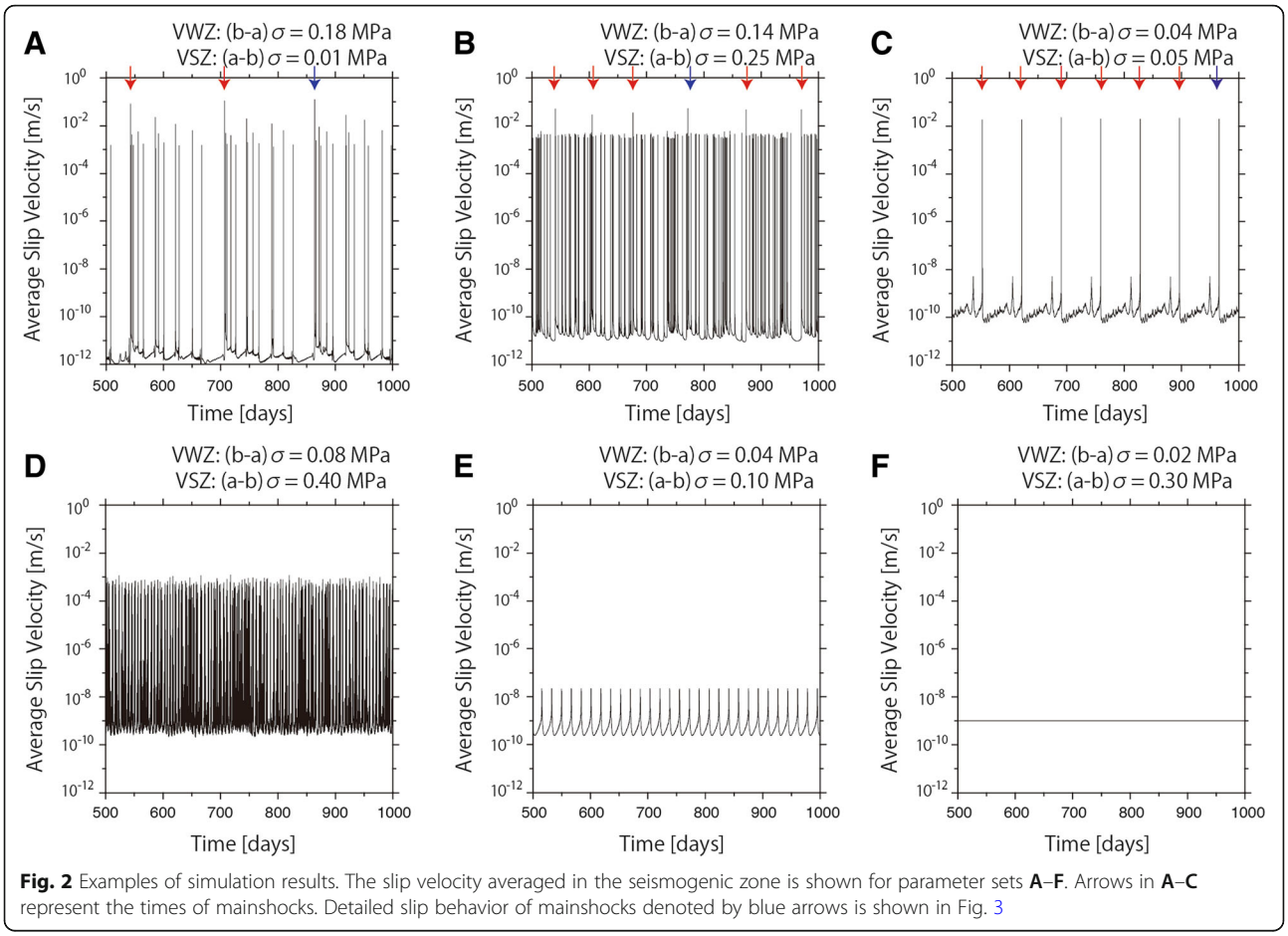

Fig. 2 Examples of simulation results. The slip velocity averaged in the seismogenic zone is shown for parameter sets **A**–**F**. Arrows in **A**–**C** represent the times of mainshocks. Detailed slip behavior of mainshocks denoted by blue arrows is shown in Fig. 3

The transition in slip behavior from the total seismic regime to the partial seismic regime corresponds to the slip behavior transitions documented by Dublanchet et al. (2013) and Yabe and Ide (2017). The transition from the total seismic regime to the slow slip regime corresponds to the slip behavior transitions documented by Skarbek et al. (2012). This transition is controlled by the spatially averaged values of frictional parameters on an infinite fault subjected to constant external stress (Yabe and Ide 2017), though the conditions of the transition vary in the finite fault system or with increasing external stress (Skarbek et al. 2012; Dublanchet et al. 2013; Luo and Ampuero 2017; Yabe and Ide 2017). In this study, we conduct parameter studies only for the a value. However, other parameters, such as cell size and the ratio of VWZ size to VSZ size, also affect the changes in the conditions of the transition. Detailed parameter studies of these changes were conducted by Luo and Ampuero (2017). Hereafter, we focus on precursory slip behavior in the total seismic regime.

Precursory behavior

Comparing the precursory slips of three examples in the total seismic regime (parameter sets A–C in Fig. 3), there are wide varieties. In parameter set A, where ξ_w is large and ψ_s is small, precursory slip is negligible and occurs only in one cell (#1). On the other hand, in parameter sets B and C, which are closer to the stability boundary between the total seismic regime and other regimes, intense precursory aseismic and seismic slip occurs across a wide area of the fault. To quantify these variations, we define the precursory period and foreshocks below, then report the relevant results for each precursory slip behavior.

During the interseismic period, the precursory period (Fig. 5a) begins at the last time when the slip velocity averaged over the seismogenic zone exceeds the plate velocity before the mainshock. The end of the precursory period (or equivalently, the beginning of the mainshock) is defined as the last time at which the average slip velocity exceeds 1 mm/s before the peak averaged slip velocity during the mainshock. Foreshock events are defined as precursory seismic events, during which the maximum average slip velocity exceeds 1 mm/s (Fig. 5b).

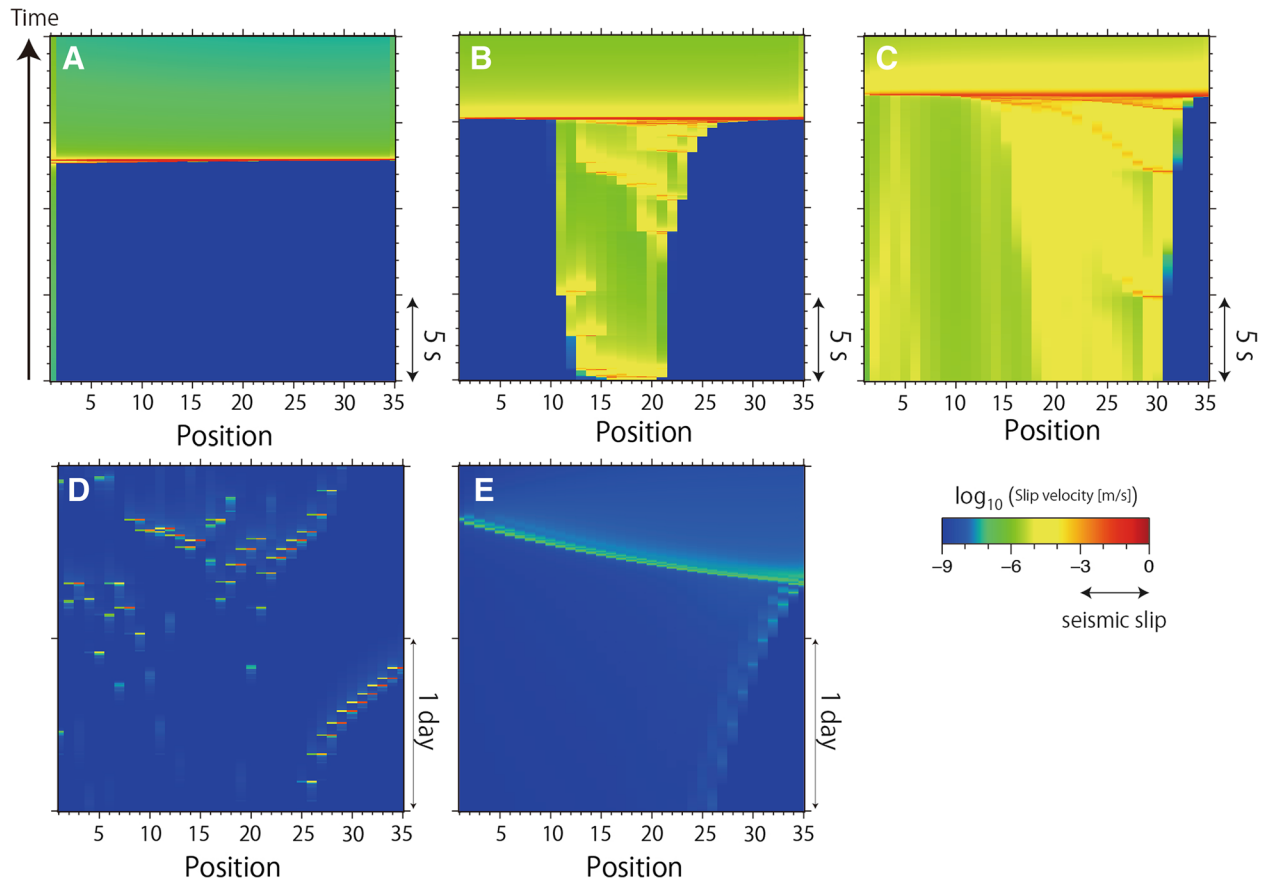

Fig. 3 Detailed slip behaviors of the fault. Five examples (parameter sets **A**–**E** in Fig. 2) are shown, one per panel. Horizontal axis shows the location (referenced by cell number) along the fault (cf. Fig. 1). Time flows from bottom to top on the vertical axis. Color intensity corresponds to slip velocity in each cell as a function of time

The first measure of the activity level of the precursory slip is the amount of aseismic slip during the nucleation process. In the case of a frictionally homogeneous fault governed by a rate- and state-dependent friction law, fault slip velocity is expected to increase proportionally to the inverse of time remaining before the mainshock

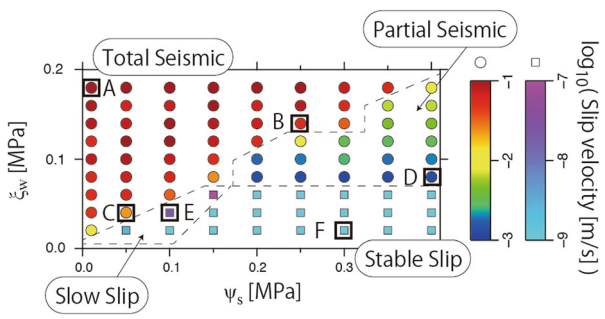

Fig. 4 Phase diagram for different types of slip behavior. Color intensity represents slip velocity. Symbols (circles and squares) denote the color scale used. The six parameter sets shown as examples in Figs. 2 and 3 are indicated by text labels **A**–**F**

(Dieterich 1992). In the case of a heterogeneous fault, the accelerated aseismic slip is expected to drive foreshocks, and the occurrence of foreshocks perturbs this simple relationship. However, it still holds true that aseismic slip velocity outside of the foreshock period accelerates in proportion to the inverse of the time before the rupture (Noda et al. 2013). Therefore, the background aseismic slip velocity V_b could be expressed as $V_b = D/t_r$, where D is a constant and t_r is the time remaining before the mainshock. The constant D (hereafter called the nucleation level) is a proxy for the amount of aseismic slip during the nucleation process. The average slip velocity is plotted against t_r as in Fig. 6a. To define the background aseismic slip velocity V_b, we need to define the slip velocity, which is not perturbed by the occurrence of foreshocks. For this purpose, we stacked the slip velocity evolutions of several precursory periods for mainshocks in Fig. 2 and measured the bottom 10th percentile value of the average slip velocity in each time bin, divided equally in log space, from 1 s before the mainshock to the beginning of the nucleation phase. Picked values of V_b were then fitted using the

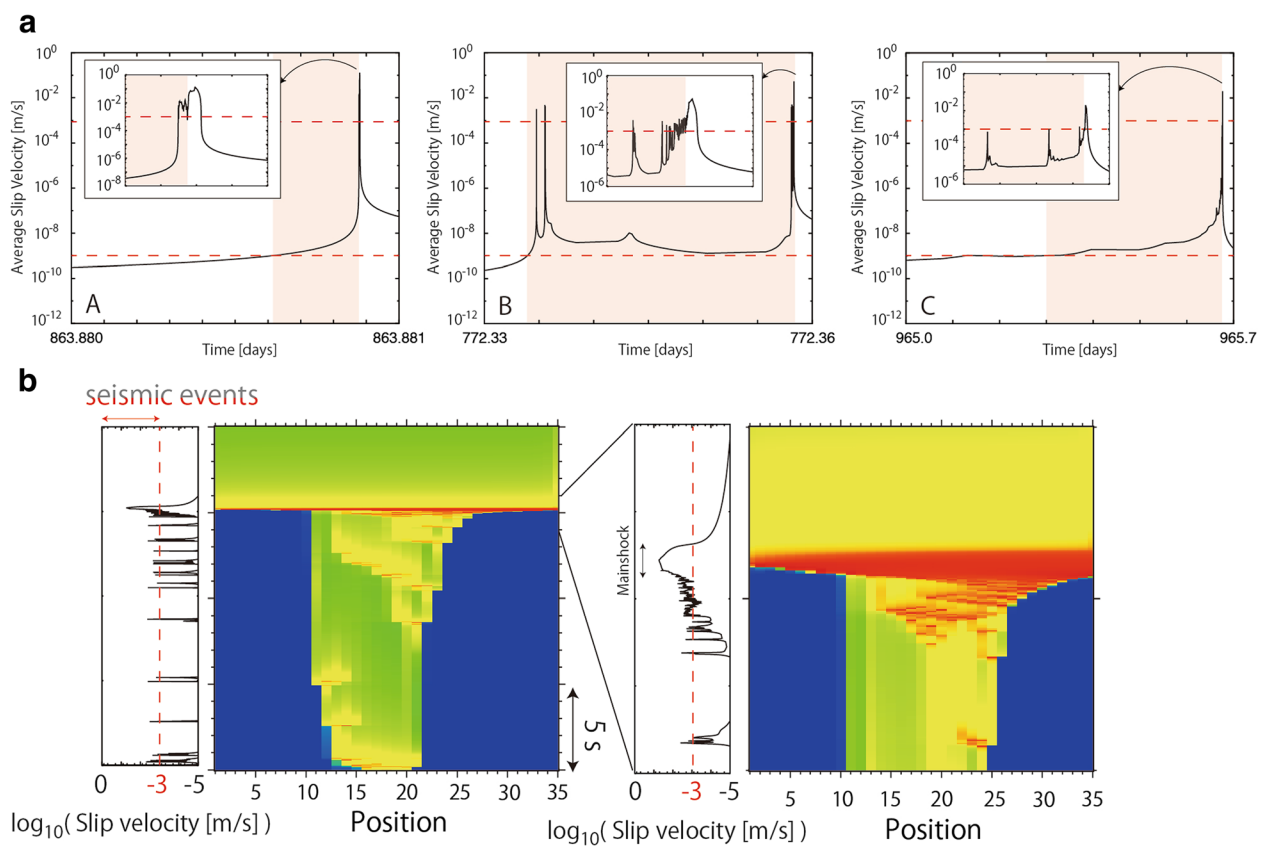

Fig. 5 Definitions of precursory periods and foreshocks. **a** Temporal evolution of average slip velocities of events for parameter sets A–C in Fig. 3. Insets show close-ups of the time periods around the mainshock. Red hatched time periods are the defined precursory periods. **b** Slip velocity distributions for parameter set B of Fig. 3 with average slip velocities. Foreshocks are defined when the average slip velocity exceeds 1 mm/s. The right panel is a close-up of the time window around the mainshock

function shape of D/t_r. This procedure was repeated for all parameter sets in the total seismic regime, and the results are summarized in Fig. 6b.

In Fig. 6a, the bottom envelopes of the slip velocity are roughly consistent with a slope of − 1, which supports our hypothesis that the background aseismic slip velocity and time to rupture are inversely proportional, even in a frictionally heterogeneous fault. The value of the nucleation level is very small for parameter set A, which indicates that the precursory slip behavior is negligible, as suggested by Fig. 3. For parameter sets B and C, the nucleation level is larger for C than for B, which indicates that aseismic slip during the nucleation is larger for C. This is also consistent with Fig. 3 because the width of the aseismic slip before the mainshock is much larger in parameter set C. The results for all parameter studies show that the nucleation level is higher around the stability boundary, though parameter sets with smaller ξ_w tend to have higher nucleation levels.

The other measurement of the activity of the precursory slip behavior is the amount of seismic slip during the precursory period. The seismic slip of foreshocks is driven by the background aseismic slip, which is quantified in Fig. 6. Such dynamic behavior is quantified by calculating the energy consumed by the radiation damping term, which mimics the energy lost by seismic wave radiation (Rice 1993). We calculate the following values using the slip velocity V_{ave} and slip x_{ave} averaged across the seismogenic zone:

$$E_{ave} = \int \frac{\mu}{2\beta} V_{ave} dx_{ave}. \tag{5}$$

The cumulative energy during the precursory period is plotted against the time remaining before the mainshock in Fig. 7a. This represents the activity of seismic slip during the precursory slip period because the energy consumption due to the radiation damping term shows a greater increase when the slip velocity is higher. The cumulative energies at 1 s before the mainshock, averaged over several precursory periods, are plotted for all parameter sets in Fig. 7b.

Because foreshocks are driven by the background aseismic slip of the nucleation process, their seismic slip

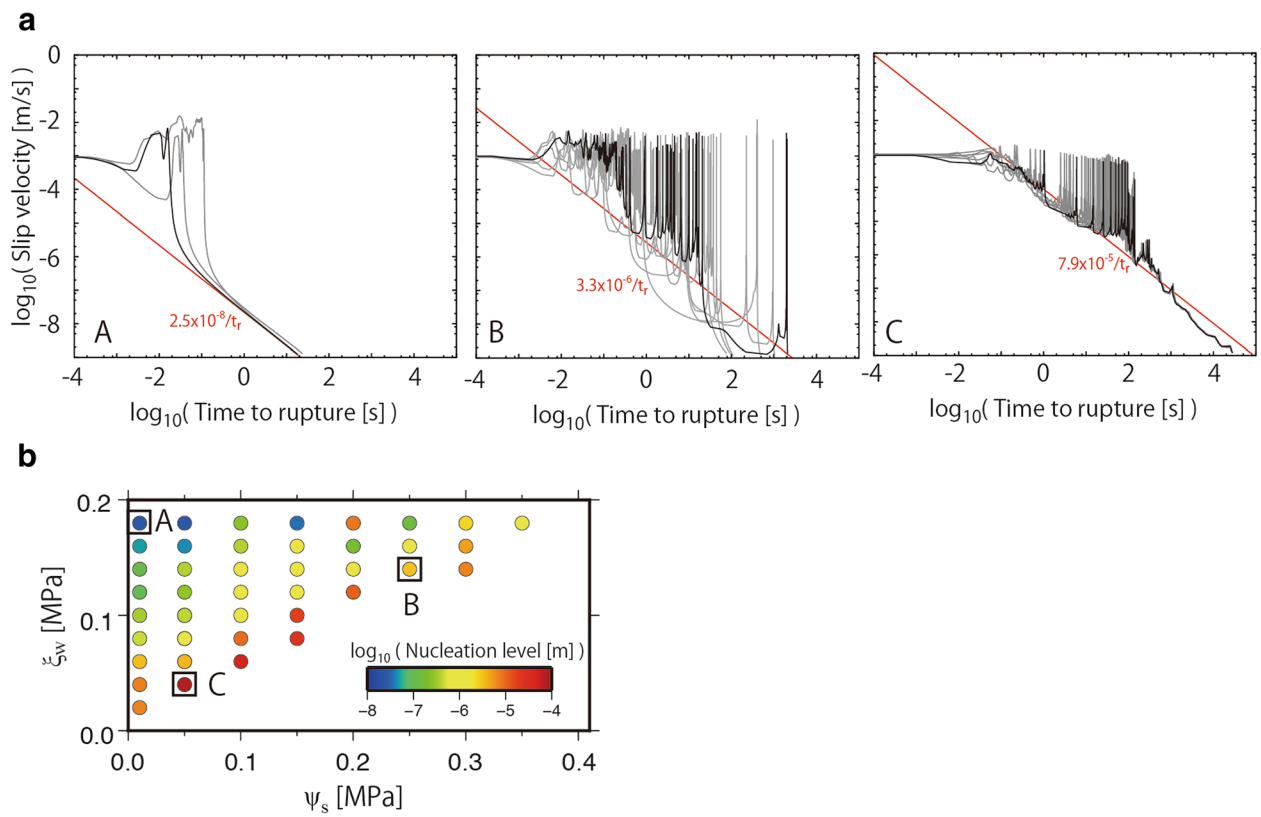

Fig. 6 Estimation of the nucleation level. **a** Average slip velocity plotted against the time remaining before the mainshock for parameter sets A–C. Black curves represent events indicated by blue arrows in Figs 2 and 3. Grey curves represent other mainshocks shown in Fig. 2. Red lines are fitted power law functions. Red text gives the estimated values of the nucleation level. **b** Results of parameter studies. The colors indicate the nucleation level *D*. Parameter sets A–C shown in **a** are denoted by squares

should be active around the stability boundary of the fault, where the background aseismic slip is most active in Fig. 6b. The cumulative energy is actually negligible for parameter set A, where the background aseismic slip is very small, but larger around the stability boundary of the fault where the background aseismic slip is also larger. Comparing parameter sets B and C, the former has larger values of cumulative energy, which indicates that seismic slip is more active during the precursory period of parameter set B. However, the nucleation level is higher in parameter set C (Fig. 6). This inconsistency between aseismic and seismic slip during the precursory period around the stability boundary of the fault should be related to the frictional parameters. The parameter set B has larger values of both ξ_w and ψ_s. A large value of ξ_w makes the nucleation size smaller and better facilitates seismic slip of individual VWZs. In contrast, parameter set C has smaller values of both ξ_w and ψ_s, which facilitates simultaneous slip across a larger region of the fault. This difference is also reflected in the amount of seismicity between mainshocks (Fig. 2), i.e., many smaller events occur between mainshocks for parameter set B, whereas no seismic events occur for parameter set C. These same tendencies should also exist in precursory slip.

Discussion

Inverse Omori law

Foreshock activity is sometimes observed before large earthquakes. Although observed foreshock seismicity varies among mainshocks, the stacked sequence of foreshocks shows power-law acceleration toward the mainshock, a so-called inverse Omori law (Kagan and Knopoff 1978; Jones and Molnar 1979). Foreshocks in our simulations are also expected to follow an inverse Omori law because foreshocks are driven by background slip, which accelerates proportionally to the inverse of the time remaining before a rupture (Fig. 6). As a demonstrative example, we measure the foreshock rate of six stacked foreshock sequences for parameter set B, where seismic slip dominates during the precursory period. We count the number of events in each time bin, which are equally distributed on a logarithmic scale. These foreshock rates are then fitted with a power law function from the beginning of the precursory slip behavior to 1 s before the mainshock, which is the same

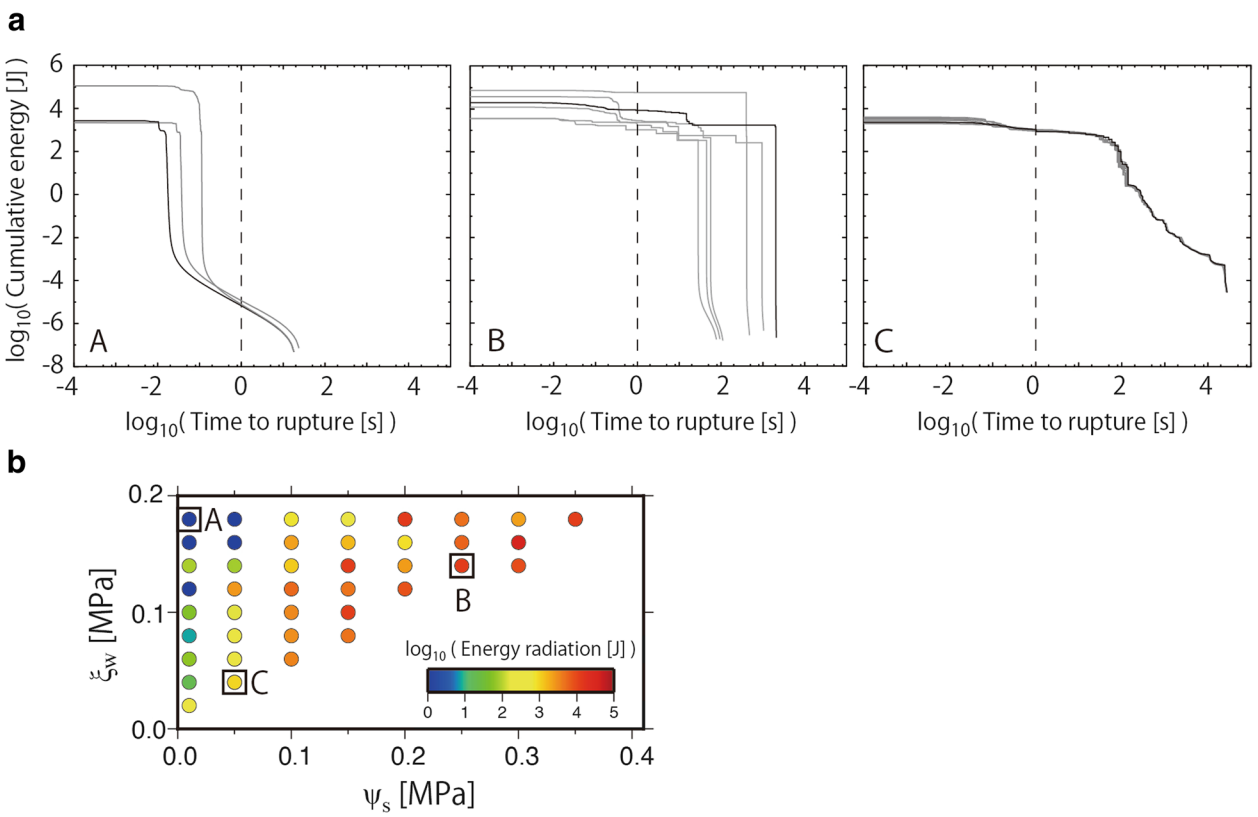

Fig. 7 Parameter studies of energy radiation. **a** Cumulative energy radiation plotted against the time remaining before the mainshock for parameter sets A–C. Black curves represent events presented in Fig. 3. Grey curves are for other mainshocks shown in Fig. 2. **b** Results of parameter studies. The color indicates the amount of cumulative energy at 1 s before the mainshock. Parameter sets A–C shown in **a** are denoted by squares

time window to which a power law function was fitted for background slip velocity in Fig. 6. Figure 8 shows the foreshock rates for the stacked sequence and the fitted power law function. The foreshock rates are well-fitted by an exponent of − 1.1. Acceleration of foreshocks on timescales of t^{-p} (with $p \sim 1$) is observed for various parameter sets with high levels of radiated seismic energy. The observation that simulated foreshocks follow an inverse Omori law is not affected by changing the definition of a foreshock from a slip velocity of 1 to 0.1 mm/s.

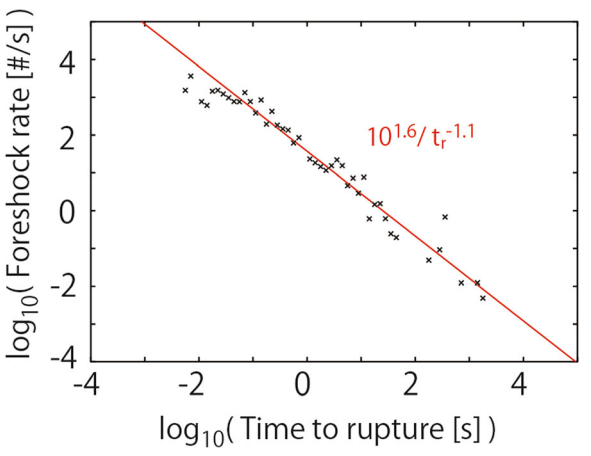

Fig. 8 Foreshock rates following an inverse Omori law. Foreshock rates measured for the stacked sequence in parameter set B are shown against the time remaining before the mainshock. The red line denotes the fitted power law function. Estimated parameters are shown in the plot with red text

Dynamic nucleation

The above quantification of precursory slip behavior reveals that precursory slip becomes intense when the frictional heterogeneity is close to the stability conditions. In addition, with parameter sets close to the stability boundary, aseismic deformation dominates more when ξ_w is smaller, whereas seismic deformation dominates more when ξ_w is larger. In contrast to the classical "static" nucleation process, where the slip velocity increases monotonically toward the mainshock, this mixture of aseismic and seismic slip during the precursory period could be called "dynamic" nucleation (Ide and Aochi 2013). Figure 9

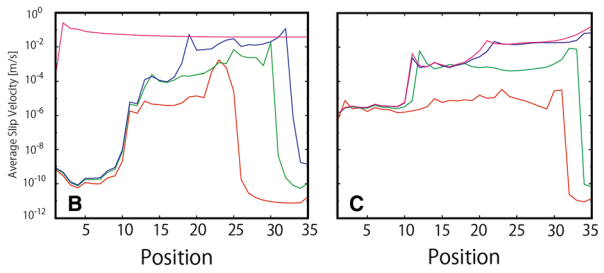

Fig. 9 Snapshots of slip velocities on the fault for parameter sets **B** and **C**. Green line shows the slip velocity at the beginning of the mainshock, when the average slip velocity exceeds 1 mm/s, corresponding to the insets in Fig. 5a. The blue and magenta lines are snapshots when the averaged slip exceeds 1 cm/s and reaches its maximum, respectively. The red line is a snapshot taken 1 s before the beginning of the mainshock

shows four snapshots of slip velocity along the fault for parameter sets B and C. In both cases, part of the seismogenic zone is accelerated toward the mainshock, which represents the nucleation zone of the fault. However, this nucleation is a result of combinations of the seismic slip of many foreshocks and aseismic slip acceleration (Fig. 6a). When the seismic slip of a foreshock is nucleated in a cell, it cannot propagate through the entire seismogenic zone during the precursory period because the accelerated zone (or nucleation zone) is not large enough to facilitate unstable slip throughout the seismogenic zone. Instead, it triggers afterslip in the cell and stress loading on surrounding cells, through coseismic and postseismic deformations. If adjacent cells were not ruptured during the precursory period, then increasing stress triggers the next foreshock. Because stress loading is greatest in the nearest neighboring cells, the precursory slip area gradually expands and the foreshocks migrate (Fig. 3). Because the fault is weakened from outside the locked area, the gradual migration of foreshocks at the front of the precursory slip area proceeds from left to right in Fig. 3. This gradual migration of the precursory slip area can also be observed in the slow-slip regime. On the other hand, if adjacent cells were ruptured during the precursory period, then the afterslip of foreshocks will be accelerated and/or another foreshock will be triggered. Because the fault is already weakened in the precursory slip area, foreshock migration is faster there than the speed at which the precursory slip area expands (Fig. 3). The fault is dynamically nucleated by the repeated occurrence of this process. When the nucleation zone grows sufficiently, after the accumulation of seismic and aseismic slip, conditions become suitable for unstable slip across the entire seismogenic zone (i.e., the mainshock).

Variations in frictional heterogeneity on the plate boundary fault

Our results show that simple frictional heterogeneity on the fault can explain the variations in activity levels of precursory slip before large earthquakes, in addition to transitions in slip behavior (Skarbek et al. 2012; Dublanchet et al. 2013; Luo and Ampuero 2017; Yabe and Ide 2017) and seismicity between mainshocks. Because frictional parameters and effective normal stresses should vary both along strike and along dip, complex seismicity in subduction zones could be explained by variations in frictional parameters. In the along-dip direction, the frictional parameter changes with depth-dependent variations in temperature and pressure (e.g., Blanpied et al. 1991). Experimental investigations of the physical properties of blueschist suggest that $a - b$ is positive at colder temperatures and lower pressures, which corresponds to the trench. This quantity becomes negative in the seismogenic zone and positive again at deeper levels (Sawai et al. 2016, 2017). Considering these tendencies, we can expect that the along-dip trajectory of frictional heterogeneity variations in Fig. 10 becomes an ellipse that extends from top-left to bottom-right in the figure.

The Nankai subduction zone hosts few interplate earthquakes in the seismogenic zone during the interseismic period, though huge earthquakes have been documented many times (Ando 1975). At the shallower and deeper extensions of the seismogenic zone, active slow earthquakes have been documented (Obara 2002; Araki et al. 2017), and the deeper plate interface slips stably. Such along-dip variations in seismicity can be explained by a conceptual model like that in Fig. 10, with an ellipse located at lower left. On the other hand, the Tohoku subduction zone hosts large numbers of small to

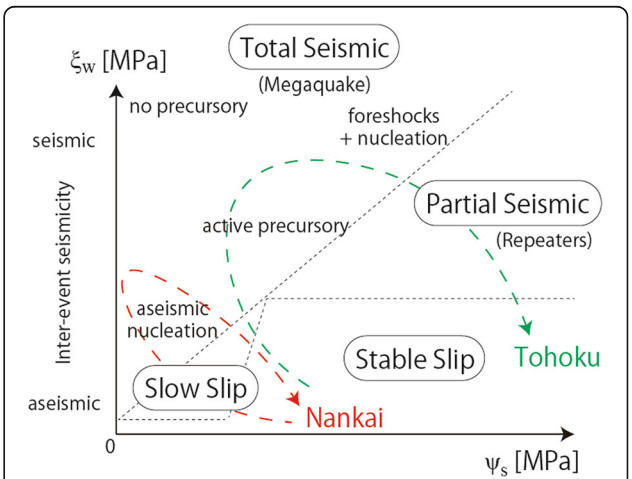

Fig. 10 Schematic phase diagram of seismicity. The two curving arrows represent along-dip variations in frictional heterogeneity in the Nankai (red) and Tohoku (green) subduction zones

moderate interplate earthquakes during the interseismic period. The existence of slow earthquakes has been documented at the shallower plate interface (Kato et al. 2012; Ito et al. 2013). Repeating earthquakes occur in deeper regions of the seismogenic zone, considered to represent isolated seismic patches on the ductile plate interface, as inferred from the observation that seismic waveforms of repeating earthquakes are highly similar (e.g., Matsuzawa et al. 2002; Igarashi et al. 2003). These along-dip variations can be explained by the conceptual model in Fig. 10 with an ellipse located in the middle. The differences between the frictional heterogeneity distributions of these two subduction zones can be explained by differences in pore fluid pressure, because dehydration reactions would be promoted by the higher temperature of the young Philippine Sea Plate subducting in the Nankai subduction zone (Peacock and Wang 1999).

Conclusions

We investigated precursory slip behavior in a frictionally heterogeneous fault using numerical simulations in which VWZs and VSZs are distributed sequentially on a finite linear fault. The activity level of the precursory slip behavior is quantified in two ways, each of which represents the activity levels of seismic and aseismic slip behavior during the precursory period. Parameter studies show that precursory slip behavior is intense when the frictional parameters are close to the fault stability boundary. Among parameter sets close to the stability boundary, aseismic slip dominates the precursory slip when ξ_w is small, whereas seismic slip dominates when ξ_w is large. Active precursory slip behavior before the mainshock could be interpreted as a type of nucleation process leading up to the mainshock, though this differs from the classical concept of nucleation in that the observed nucleation process is a mixture of the acceleration of background slip velocity and the occurrence of small seismic events. Complex seismicity modeled by a simple frictional heterogeneity can explain the along-dip and among-subduction-zone variations in observed seismicity in a qualitative way.

Abbreviations

RSF: Rate- and state-dependent friction; VSZ: Velocity-strengthening zone; VWZ: Velocity-weakening zone

Acknowledgements

Numerical simulations were conducted using the computer systems of the Earthquake and Volcano Information Center of the Earthquake Research Institute, the University of Tokyo. Figures in this manuscript were produced using the Generic Mapping Tools software package (Wessel and Smith 1998).

Funding

This study was supported by a Management Expenses Grant from the Japan Agency for Marine-Earth Science and Technology (JAMSTEC) and JSPS KAKENHI Grant Numbers JP16H02219 and JP16H06477.

Availability of data and materials

Please contact the corresponding author regarding requests for data.

Authors' contributions

SY planned the study and conducted numerical simulations. All authors contributed to the interpretations of data and preparation of the manuscript. Both authors read and approved the final manuscript.

Competing interests

The authors declare that they have no competing interests.

Publisher's Note

Springer Nature remains neutral with regard to jurisdictional claims in published maps and institutional affiliations.

Author details

[1]Department of Solid Earth Geochemistry, Japan Agency for Marine-Earth Science and Technology, 2-15, Natsushima-cho, Yokosuka, Kanagawa 237-0061, Japan. [2]Department of Earth and Planetary Science, University of Tokyo, 7-3-1 Hongo, Bunkyo, Tokyo 113-0033, Japan.

Received: 15 March 2018 Accepted: 3 August 2018
Published online: 22 August 2018

References

Abercrombie RE, Mori J (1996) Occurrence patterns of foreshocks to large earthquakes in the western United States. Nature 381:303–307. https://doi.org/10.1038/381303a0

Ando M (1975) Source mechanisms and tectonic signi cance of historical earthquakes along the Nankai Trough, Japan. Tectonophysics 27:119–140. https://doi.org/10.1016/0040-1951(75)90102-X

Ando R, Imanishi K (2011) Possibility of Mw 9.0 main shock triggered by diffusional propagation of after-slip from Mw 7.3 foreshock. Earth Planets Space 63:767–771. https://doi.org/10.5047/eps.2011.05.016

Araki E, Saffer DM, Kopf AJ, Wallace LM, Kimura T, Machida Y, Ide S, Davis E, IODP Expedition 365 shipboard sciencets (2017) Recurring and triggered slow-slip events near the trench at the Nankai trough subduction megathrust. Science 356:1157–1160. https://doi.org/10.1126/science.aan3120

Beeler NM, Thomas A, Bürgmann R, Shelly D (2013) Inferring fault rheology from low-frequency earthquakes on the San Andreas. J Geophys Res 118:5976–5990. https://doi.org/10.1002/2013JB010118

Beroza GC, Zoback MD (1993) Mechanism diversity of the Loma Prieta aftershocks and the mechanics of mainshock-aftershock interaction. Science 259:210–213. https://doi.org/10.1126/science.259.5092.210

Blanpied ML, Lockner DA, Byedee JD (1991) Fault stability inferred from granite sliding experiments at hydrothermal conditions. Geophys Res Lett 18(4):609–612. https://doi.org/10.1029/91GL00469

Bouchon M, Durand V, Marsan D, Karabulut H, Schmittbuhl J (2013) The long precursory phase of most large interplate earthquakes. Nat Geosci 6:299–302. https://doi.org/10.1038/ngeo1770

Bouchon M, Karabulut H, Aktar M, Ozalaybey S, Schmittbuhl J, Bouin MP (2011) Extended nucleation of the 1999 Mw 7.6 Izmit earthquake. Science 331:877–880. https://doi.org/10.1126/science.1197341

Dieterich JH (1979) Modeling of rock friction: 1. Experimental results and constitutive equations. J Geophys Res 84(B5):2161–2168. https://doi.org/10.1029/JB084iB05p02161

Dieterich JH (1992) Earthquake nucleation on faults with rate-and state-dependent strength. Tectonophysics 211:115–134. https://doi.org/10.1016/0040-1951(92)90055-B

Dodge DA, Beroza GC, Ellsworth WL (1995) Foreshock sequence of the 1992 Landers, California, earthquake and its implications for earthquake nucleation. J Geophys Res 100:9865–9880. https://doi.org/10.1029/95JB00871

Dodge DA, Beroza GC, Ellsworth WL (1996) Detailed observations of California foreshock sequence: implications for the earthquake initiation process. J Geophys Res 101(B10):22371–22392. https://doi.org/10.1029/96JB02269

Dublanchet P, Bernard P, Favreau P (2013) Interactions and triggering in a 3-D rate-and-state asperity model. J Geophys Res 118:2225–2245. https://doi.org/10.1002/jgrb.50187

Fagereng Å, Hillary GWB, Diener JFA (2014) Brittle-viscous deformation, slow slip, and tremor. Geophys Res Lett 41:4159–4167. https://doi.org/10.1002/2014GL060433

Fagereng Å, Sibson RH (2010) Mélange rheology and seismic style. Geology 38(8):751–754. https://doi.org/10.1130/G30868.1
Fehlberg E (1969) Low-order classical Runge–Kutta formulas with step size control and their application to some heat transfer problems. NASA Technical Report 315
Helmstetter A, Sornette D (2003a) Foreshocks explained by cascades of triggered seismicity. J Geophys Res 108(B10):2457. https://doi.org/10.1029/2003JB002409
Helmstetter A, Sornette D (2003b) Båth's law derived from the Gutenberg-Richter law and from aftershock properties. Geophys Res Lett 30(20):2069. https://doi.org/10.1029/2003GL018186
Helmstetter A, Sornette D, Grasso JR (2003) Mainshocks are aftershocks of conditional foreshocks: how do foreshock statistical properties emerge from aftershock laws. J Geophys Res 108(B1):2046. https://doi.org/10.1029/2002JB001991
Houston H (2015) Low friction and fault weakening revealed by rising sensitivity of tremor to tidal stress. Nat Geosci 8:409–415. https://doi.org/10.1038/ngeo2419
Ide S, Aochi H (2013) Historical seismicity and dynamic rupture process of the 2011 Tohoku-Oki earthquake. Tectonophysics 600:1–13. https://doi.org/10.1016/j.tecto.2012.10.018
Ide S, Tanaka Y (2014) Controls on plate motion by oscillating tidal stress: evidence from deep tremors in western Japan. Geophys Res Lett 41:3842–3850. https://doi.org/10.1002/2014GL060035
Igarashi T, Matsuzawa T, Hasegawa A (2003) Repeating earthquakes and interplate aseismic slip in the northeastern Japan subduction zone. J Geophys Res 108(B5):2249. https://doi.org/10.1029/2002JB001920
Ito Y, Hino R, Kido M, Fujimoto H, Osada Y, Inazu D, Ohta Y, Iinuma T, Ohzono M, Miura S, Mishina M, Suzuki K, Tsuji T, Ahi J (2013) Episodic slow slip events in the Japan subduction zone before the 2011 Tohoku-Oki earthquake. Tectonophysics 600:14–26. https://doi.org/10.1016/j.tecto.2012.08.022
Jones LM, Molnar T (1979) Some characteristics of foreshocks and their possible relationship to earthquake prediction and premonitory slip on faults. J Geophys Res 84(B7):3596–3608. https://doi.org/10.1029/JB084iB07p03596
Kagan Y, Knopoff L (1978) Statistical study of the occurrence of shallow earthquakes. Geophys J Int 55:67–86. https://doi.org/10.1111/j.1365-246X.1978.tb04748.x
Kato A, Obara K, Igarashi T, Tsuruoka H, Nakagawa S, Hirata N (2012) Propagation of slow slip leading up to the 2011 Mw 9.0 Tohoku-Oki earthquake. Science 335(6069):705–708. https://doi.org/10.1126/science.1215141
Luo Y, Ampuero JP (2017) Stability of faults with heterogeneous friction properties and effective normal stress. Tectonophysics. https://doi.org/10.1016/j.tecto.2017.11.006
Matsuzawa T, Igarashi T, Hasegawa A (2002) Characteristic small-earthquake sequence off Sanriku, northeastern Honshu, Japan. Geophys Res Lett 29(11). https://doi.org/10.1029/2001GL014632
McGuire JJ, Boettcher MS, Jordan TH (2005) Foreshock sequences and short-term earthquake predictability on East Pacific Rise transform faults. Nature 434:457–461. https://doi.org/10.1038/nature03377
McLaskey GC, Kilgore BD (2013) Foreshocks during the nucleation of stick-slip instability. J Geophys Res Solid Earth 118:2982–2997. https://doi.org/10.1002/jgrb.50232
Miyazawa M, Brodsky EE (2008) Deep low-frequency tremor that correlates with passing surface waves. J Geophys Res 113:B01307. https://doi.org/10.1029/2006JB004890
Noda H, Nakatani M, Hori T (2013) Large nucleation before large earthquakes is sometimes skipped due to cascade-up—implications from a rate and state simulation of faults with hierarchical asperities. J Geophys Res Solid Earth 118:2924–2952. https://doi.org/10.1002/jgrb.50211
Obara K (2002) Nonvolcanic deep tremor associated with subduction in southwest Japan. Science 296(5573):1679–1681. https://doi.org/10.1126/science.1070378
Ogata Y (1988) Statistical models for earthquake occurrence and residual analysis for point processes. J Am Stat Assoc 83:9–27
Peacock SM, Wang K (1999) Seismic consequences of warm versus cool subduction metamorphism: examples from southwest and northeast Japan. Science 286:937–939. https://doi.org/10.1126/science.286.5441.937
Rice JR (1993) Spatio-temporal complexity of slip on a fault. J Geophys Res 98(B6):9885–9907. https://doi.org/10.1029/93JB00191
Rubin AM, Ampuero JP (2005) Earthquake nucleation on (aging) rate and state faults. J Geophys Res 110:B11312. https://doi.org/10.1029/2005JB003686
Ruiz S, Metois M, Fuenzalida A, Ruiz J, Leyton F, Grandin R, Vigny C, Madariaga R, Campos J (2014) Intense foreshocks and a slow slip event preceded the 2014 Iquique Mw 8.1 earthquake. Science 345(6201):1165–1169. https://doi.org/10.1126/science.1256074
Sawai M, Niemeijer AR, Hirose T, Spiers CJ (2017) Frictional properties of JFAST core samples and implications for slow earthquakes at the Tohoku subduction zone. Geophys Res Lett 44:8822–8831. https://doi.org/10.1002/2017GL073460
Sawai M, Niemeijer AR, Plümper O, Hirose T, Spiers CJ (2016) Nucleation of frictional instability caused by fluid pressurization in subducted blueschist. Geophys Res Lett 43:2543–2551. https://doi.org/10.1002/2015GL067569
Skarbek RM, Rempel AW, Schmidt DA (2012) Geologic heterogeneity can produce aseismic slip transients. Geophys Res Lett 39:L21306. https://doi.org/10.1029/2012GL053762
Thomas MY, Lapusta N, Noda H, Avouac J-P (2014) Quasi-dynamic versus fully dynamic simulations of earthquakes and aseismic slip with and without enhanced coseismic weakening. J Geophys Res Solid Earth 119:1986–2004. https://doi.org/10.1002/2013JB010615
Ujiie K, Saishu H, Fagereng Å, Nishiyama N, Otsubo M, Masuyama H, Kagi H (2018) An explanation of episodic tremor and slow slip constrained by crack-seal veins and viscous shear in subduction mélange. Geophys Res Lett 45. https://doi.org/10.1029/2018GL078374
Wessel P, Smith WHF (1998) New, improved version of generic mapping tools released. Eos Trans AGU 79(47):579. https://doi.org/10.1029/98EO00426
Wibberley CAJ, Shimamoto T (2003) Internal structure and permeability of major strike-slip fault zones: the Median Tectonic Line in Mie Prefecture, Southwest Japan. J Struct Geol 25(1):59–78. https://doi.org/10.1016/S0191-8141(02)00014-7
Woessner J, Schorlemmer D, Wiemer S, Mai PM (2006) Spatial correlation of aftershock locations and on-fault main shock properties. J Geophys Res 111:B08301. https://doi.org/10.1029/2005JB003961
Yabe S, Ide S (2017) Slip-behavior transitions of a heterogeneous linear fault. J Geophys Res Solid Earth 122:387–410. https://doi.org/10.1002/2016JB013132
Yabe S, Ide S (2018) Why do aftershocks occur within the rupture area of a large earthquake? Geophys Res Lett 45. https://doi.org/10.1029/2018GL077843
Yabe S, Tanaka Y, Houston H, Ide S (2015) Tidal sensitivity of tectonic tremors in Nankai and Cascadia subduction zones. J Geophys Res Solid Earth 120:7587–7605. https://doi.org/10.1002/ 2015JB012250

Submit your manuscript to a SpringerOpen journal and benefit from:

► Convenient online submission
► Rigorous peer review
► Open access: articles freely available online
► High visibility within the field
► Retaining the copyright to your article

Submit your next manuscript at ► springeropen.com